High-K three-quasiparticle isomers in the proton-rich nucleus ^{129}Nd

C. M. Petrache,[1,*] J. Uusitalo,[2,3] A. D. Briscoe,[3,2] C. M. Sullivan,[3] D. T. Joss,[3] H. Tann,[2,†] Ö. Aktas,[4] B. Alayed,[3] M. A. M. Al-Aqeel,[3] A. Astier,[1] H. Badran,[2] B. Cederwall,[4] C. Delafosse,[2,‡] A. Ertoprak,[4] Z. Favier,[1,§] U. Forsberg,[2,¶] W. Gins,[2] T. Grahn,[2] P. T. Greenlees,[2] X. T. He,[5] J. Heery,[2,**] J. Hilton,[2,†] S. Kalantan,[3] R. Li,[1] P. M. Jodidar,[1] R. Julin,[2] S. Juutinen,[2] M. Leino,[2] M. C. Lewis,[3] J. G. Li,[6] Z. P. Li,[7] M. Luoma,[2] B. F. Lv,[6] A. McCarter,[3] S. Nathaniel,[3] J. Ojala,[2] R. D. Page,[3] J. Pakarinen,[2] P. Papadakis,[8,††] E. Parr,[3,‡‡] J. Partanen,[2,§§] E. S. Paul,[3] P. Rahkila,[2] P. Ruotsalainen,[2] M. Sandzelius,[2] J. Sarén,[2] J. Smallcombe,[3] J. Sorri,[9,¶¶] S. Szwec,[2,***] L. J. Wang,[7] Y. Wang,[5] L. Waring,[3] F. R. Xu,[10] J. Zhang,[5] Z. H. Zhang,[11] K. K. Zheng,[6] and G. Zimba[2]

[1] *Université Paris-Saclay, CNRS/IN2P3, IJCLab, 91405 Orsay, France*
[2] *Accelerator Laboratory, Department of Physics, University of Jyväskylä, FI-40014 Jyväskylä, Finland*
[3] *Oliver Lodge Laboratory, Department of Physics, University of Liverpool, Liverpool L69 7ZE, United Kingdom*
[4] *KTH Department of Physics, S-10691 Stockholm, Sweden*
[5] *College of Materials Science and Technology, Nanjing University of Aeronautics and Astronautics, Nanjing 210016, China*
[6] *Key Laboratory of High Precision Nuclear Spectroscopy and Center for Nuclear Matter Science, Institute of Modern Physics, Chinese Academy of Sciences, Lanzhou 730000, People's Republic of China*
[7] *School of Physical Science and Technology, Southwest University, Chongqing 400715, China*
[8] *University of Jyväskylä, Department of Physics, P.O. Box 35, FI-40014 University of Jyväskylä, Finland*
[9] *Sodankylä, Geophysical Observatory University of Oulu, FIN-99600 Sodankylä, Finland*
[10] *State Key Laboratory of Nuclear Physics and Technology, School of Physics, Peking University, Beijing 100871, China*
[11] *Mathematics and Physics Department, North China Electric Power University, Beijing 102206, China*

Three three-quasiparticle isomers, one at an excitation energy of 2.3 MeV with $T_{1/2} = 0.48(4)$ μs, and two shorter-lived with unknown half-lives at slightly lower energies have been identified in ^{129}Nd using the MARA + JUROGAM 3 setup and the recoil tagging technique. All three isomers present decay patterns characteristic of high-K isomers. The known 6.7 s β-decaying isomer previously assigned to the $5/2^+$ level is now assigned to the new $7/2^-$ ground state. A new low-spin $5/2^+$ isomeric state with a half-life of a few tens of nanoseconds has been identified, while a previously known 2.6 s β-decay activity was assigned to the band head of the $\nu 1/2^+[411]$ band. The transitions depopulating the high-K isomers to low-lying states also establish the relative energies of three low-lying one-quasiparticle bands, leading to a new spin-parity assignment of $7/2^-$ to the ground state of ^{129}Nd. The partial half-lives of the depopulating transitions suggest spin-parities $21/2^+$, $19/2^+$ and $17/2^+$ for the three high-K isomers. The properties of the band built on the $21/2^+$ isomeric state suggest a one neutron-two proton configuration. Based on the results of extensive calculations with different models, we also assign one neutron - two proton configurations to the $19/2^+$ and $17/2^+$ isomeric states. The assigned configurations of the $17/2^+$ and $21/2^+$ isomeric states involve the $\pi 9/2^+[404]$ orbital, which is for the first time identified in three-quasiparticle bands of proton-rich $A \approx 130$ nuclei.

PACS numbers: 21.10.Re, 21.60.Ev, 23.20.Lv, 27.60.+j

I. INTRODUCTION

Exploring and extending the nuclear chart towards the limits of stability is one of the main endeavors in nuclear structure. Experiments devoted to the study of extremely proton-rich nuclei by employing radioactive and

*Corresponding author: petrache@ijclab.in2p3.fr
†Present address: Oliver Lodge Laboratory, Department of Physics, University of Liverpool, Liverpool L69 7ZE, United Kingdom
‡Present address: Université Paris-Saclay, CNRS/IN2P3, IJCLab, 91405 Orsay, France
§Present address: Irfu, CEA, Universit Paris-Saclay, F-91191 Gif-sur-Yvette, France
¶Present address: Department of Physics, University of York, Heslington, York YO10 5DD, United Kingdom; Present address: Department of Physics, Lund University, SE-22100 Lund, Sweden
**Present address: Department of Physics, University of Surrey, Guildford, Surrey GU2 7XH, United Kingdom
††Present address: STFC Daresbury Laboratory, Daresbury, Warrington WA4 4AD, UK
‡‡Present address: GSI Helmholtzzentrum fr Schwerionenforschung GmbH, 64291 Darmstadt, Germany
§§Deceased
¶¶Radiation and Nuclear Safety Authority in Finland Jokiniemenkuja 1, 01370 Vantaa
***Helsinki Institute of Physics, University of Helsinki, FIN-00014 Helsinki, Finland

stable-ion beams, as well as powerful setups composed of recoil mass spectrometers or projectile fragment separators, with high-efficiency arrays for detection of γ-rays and charged particles at the entrance and at the focal plane of the spectrometers. A wide field of investigation remains yet unexplored with stable projectile-target combinations using newly developed instruments which have much higher sensitivity. Such studies with stable-ion beams have been recently performed with the MARA + JUROGAM 3 setup [1–3] in the $A \approx 120$ mass region, revealing extremely rich band structures in the light ^{119,120}Ba and ^{118,119}Cs nuclei, and phenomena unexpected in this mass region, like shape coexistence, chiral bands or octupole correlations [4–9].

The present experiment, devoted to the study of nuclei with $Z > 56$, reports the discovery of three high-K isomers, one low-spin isomer, and a new spin-parity assignment to the ground state in ^{129}Nd. From the comparison of the experimental data with configuration-constrained potential energy surfaces (CC-PES) [10], projected shell model (PSM) [11], and particle number conserving cranked shell model (PNC-CSM) [12] calculations, we assign one neutron-two proton configurations to the high-spin isomers, two of them involving the $\pi 9/2^+[404]$ orbital. These are the first reported multi-quasiparticle high-K isomers involving the $\pi 9/2[404]$ orbital in $A \approx 130$ nuclei, which previously were only observed in one-quasiparticle bands close to the ground state of odd-even and odd-odd nuclei like the neighboring Pr nuclei (see e. g. [13]), and in odd-even nuclei just above the $Z = 50$ closed shell [14–21]. No high-K isomers are known in the well studied Nd nuclei with $N \leq 73$ [22–27], while high-K isomers with spins 8^- and 7^- built on two-neutron configurations are known in $N = 74$ and $N = 72$ isotopes, respectively (see e. g. [28]). The ^{129}Nd nucleus was previously investigated using the ^{92}Mo(^{40}Ca,$\alpha 2pn$) fusion-evaporation reaction [29] and the β-decay of ^{129}Pm [30]. Four rotational structures observed up to very high spin have been identified in Ref. [29], and configurations have been assigned based on the measured $B(M1)/B(E2)$ ratios, aligned angular momenta, band crossings and signature splitting and cranked shell model calculations. A 2.3 s isomer was identified by bombarding a ^{96}Ru target with a ^{36}Ar beam and using helium-jet fast tape transport system to measure the β-decay of ^{129}Pm [30].

II. EXPERIMENTAL DETAILS AND RESULTS

In the present work, highly excited ^{129}Nd nuclei have been produced using the ^{58}Ni(^{78}Kr,$\alpha 2pn$) fusion-evaporation reaction. The ^{78}Kr beam was provided by the K130 Cyclotron at the University of Jyväskylä, Finland. The target was a 750 μg/cm^2 thick self-supporting foil of enriched ^{58}Ni. Two experiments have been performed. One without JUROGAM 3 to search for β-delayed proton emitters, lasting for 10 days with several beam energies between 340 MeV and 370 MeV, and a second one lasting 4 days, in which JUROGAM 3 was added and the beam energy of 364 MeV was optimized for the production of ^{129}Nd. The in-flight double-focusing recoil mass separator MARA [1, 31] was tuned for mass 133 for the low beam energies (half of the beam time), allowing the observation of mass 129 which fully overlapped with mass 133 due to an A/q ambiguity. The flight time of the recoils from target to the implantation point is ≈ 450 ns. At the target position, the particle detector array JYUTube consisting of 96 separate scintillator detectors with SiPM (Silicon Photo Multiplier) readouts was used for charged particle identification. In the second experiment in which the beam energy of 364 MeV was optimized for ^{129}Nd, the MARA separator was tuned for mass 129, with the aim to search for the prompt γ rays which feed the isomeric states in ^{129}Nd using the recoil gated isomer tagging technique. Prompt γ-rays were detected at the target position using the JUROGAM 3 germanium-detector array consisting of 24 Euroball clover [32] and 15 Eurogam Phase I-type [33] escape-suppressed detectors, with an efficiency of $\approx 5\%$ at 1.3 MeV. The clover detectors were arranged symmetrically relative to a plane perpendicular to the beam direction (twelve at 75.5° and twelve at 104.5°), while the Phase I detectors were placed at backward angles with respect to the beam direction (five at 157.6° and ten at 133.6°). JYUtube was not in use.

The fusion-evaporation residues were separated as a function of A/q and identified using the MARA separator. At the focal plane a position-sensitive Multi-Wire-Proportional Counter (MWPC) was used to obtain A/q spectra. Part of the time a double-mass slit system was used to allow only two charge states of a given mass to be transported into the implantation detector, a 300 μm thick Double-Sided-Silicon-strip Detector (DSSD) placed 40 cm behind the MWPC. Behind the DSSD a second layer of silicon detectors (500 μm thick) is used to veto punch-through events. The Time-of Flight (ToF) between the MWPC and DSSD is recorded. The ToF and the recoil energy deposited in the DSSD were used to distinguish between fusion recoils and scattered beam. Five clover germanium detectors surrounding the MARA focal-plane detection system were used to detect γ rays emitted from long-lived isomeric states and daughters of the β decays of the implanted recoils. All detector signals were recorded by the triggerless Total Data Readout (TDR) data acquisition system, and time stamped by a global 100 MHz clock, which allowed the establishment of both temporal and spatial correlations between recoils and events obtained with the remaining detectors of the focal plane and of the JUROGAM 3 arrays [2, 34].

The data were sorted into coincidence $\gamma\gamma$ matrices and $\gamma\gamma\gamma$ cubes, and analyzed using the GRAIN [35] and RADWARE [36, 37] packages. In the first part of the analysis new delayed transitions in coincidence with low-lying transitions already known in the one-quasiparticle bands of ^{129}Nd were identified at the focal plane. Then in the

second part, γ- and recoil-gated prompt spectra measured in JUROGAM 3 were constructed to identify transitions above the isomers. The multipolarities and the mixing ratios of the newly identified γ-ray transitions were established based on angular correlations data.

Figure 1 shows a partial level scheme of ^{129}Nd, with the previously known bands [29] drawn in black, and the new transitions drawn in red. Three high-K isomeric states have been identified, with excitation energies of 1893, 2109 and 2284 keV, and spin-parity assignments of $17/2^+$, $19/2^+$ and $21/2^+$, respectively, discussed in the following. The prompt-delayed $\gamma\gamma$ coincidence spectrum of Fig. 2, obtained by gating on the 848-keV transition depopulating the 2284-keV, $21/2^+$ state and on the 551-keV transition of Band 4 detected at the MARA focal plane, shows a series of prompt transitions which have been grouped in the newly observed Band 5. Spectra of delayed transitions measured at the MARA focal plane, obtained by gating on transitions depopulating the $21/2^+$ isomeric state and presenting transitions in the lower part of the known one-quasiparticle bands are shown in Fig. 3. A singles γ-ray spectrum, and a projection of the $\gamma\gamma$ matrix measured with the germanium detectors at the focal plane of the MARA separator are shown in Fig. 4. They give an overall view of the relative intensity of the transitions depopulating the isomers, with the 848-keV transition being the strongest. Figure 5 shows two focal plane spectra obtained from the $\gamma\gamma$ matrix by gating on the 175- and 391-keV transitions which depopulate the $21/2^+$ isomer to the lower-lying $19/2^+$ and $17/2^+$ isomers, respectively. The non-observation of the transitions depopulating the $17/2^+$ isomer in the spectrum gated by the 175-keV transition indicates the missing 216-keV connecting transition between the $19/2^+$ and $17/2^+$ isomers, giving thus support to the assignment of very different configurations to the two isomers.

The experimental information on the transitions depopulating the three high-K isomers is given in Table I.

The half-life of the $21/2^+$ isomeric state has been extracted from the summed time spectra between the DSSD and the germanium detectors at the focal plane of MARA, by gating on the strong and clean 848- and 551-keV transitions. A value of $T_{1/2} = 0.48(4)$ μs has been determined from the fit of the time spectrum with two exponential functions, the one with long half-life being necessary to account for random coincidences (see Fig. 6).

Six transitions depopulating the $21/2^+$ isomeric state have been identified: four of 537, 796, 848 and 1050 keV to Bands 1, 3 and 4, and two of 391 and 175 keV to the $17/2^+$ and $19/2^+$ isomeric states, respectively, which in turn decay to low-lying states of Bands 1 and 4 via ten transitions of 566, 659, 672, 740, 823, 924, 955, 1009, 1138 and 1183 keV (see Fig. 4).

III. DISCUSSION

A. Spin-parity and configuration assignments to the isomers

One of the key issues is the assignment of spins and parities to the observed isomers. This was done by analyzing the observed decay out patterns of the isomers, including the $logF_W$ [38] values of the depopulating transitions, the single-particle aligned angular momentum i_x, kinematic moment of inertia $J^{(1)}$ and total angular momentum on the rotation axis J_x of the band built on the 2284-keV isomeric state (see Fig. 7). In addition, the assumption widely employed in high-spin region of well deformed nuclei that the spin increases with increasing excitation energy is adopted. Figure 7 shows the experimental single-particle aligned angular momenta of the bands built on the $21/2^+$ isomer in ^{129}Nd and on the 8^- isomers in the $N = 74$ nuclei, the kinematic moment of inertia $J^{(1)}$, and the total angular momentum on the rotation axis J_x of the one-quasiparticle Band 1 and of the three-quasiparticle Band 5 built on the 2284-keV isomer.

Based on the lowest and highest spins of the states fed by the isomers, we concluded that their spins have to be between 17/2 and 21/2. The spin-parity of the 2284-keV isomeric state can be either $17/2^{\pm}$, $19/2^{\pm}$ or $21/2^+$. The $17/2^{\pm}$ and $19/2^-$ assignments can be discarded because they would lead to transitions increasing spin by $1\hbar$ for the $17/2^+$ assignment ($17/2^+ \rightarrow 19/2^+$ to Band 4 and $19/2^+ \rightarrow 21/2^-$ from the 2109-keV isomeric state to Band 1), or $2\hbar$ for the $17/2^-$ and $19/2^-$ assignments ($15/2^- \rightarrow 19/2^+$ from the 1893-keV isomeric state to Band 4), which are unlikely in the de-excitation of high-spin states.

The candidate configurations of the remaining $19/2^+$ and $21/2^+$ possible assignments can be established from the analysis of the single-particle alignment and crossing frequency of the band built on the isomer. As one can see in Fig. 7, Band 5 above the 2284-keV isomeric state consists of two completely degenerate signature partners and has $i_x \approx 1.5\hbar$, indicating the presence of only high-Ω orbitals in its configuration. The upbend at a rotational frequency of $\hbar\omega \approx 0.35$ MeV observed in all one-quasiparticle bands of ^{129}Nd (see Fig. 6 of Ref. [29] and in Fig. 7) and in the bands built on the 8^- isomers with two-neutron configurations of the $N = 74$ isotones, all attributed to the alignment of a pair of $h_{11/2}$ protons, is absent in Band 5. With the $(\pi h_{11/2})^2$ alignment being blocked, the configuration has to involve one $h_{11/2}$ proton orbital, which can be either $\pi 5/2^-[532]$ or $\pi 3/2^-[541]$. For $Z = 60$ and $\varepsilon_2 \approx 0.3$, the Fermi surface is in the middle of the $h_{11/2}$ sub-shell where the $\pi 5/2^-[532]$ Nilsson orbital is closest in energy, being therefore favored. To establish the orbital occupied by the second proton in the isomer configuration, we observe that $J^{(1)}$ of Band 5 is smaller than that of Band 1 above the upbending, where two rotationally aligned $h_{11/2}$ protons are present, suggesting that the second proton occupies a high-Ω or-

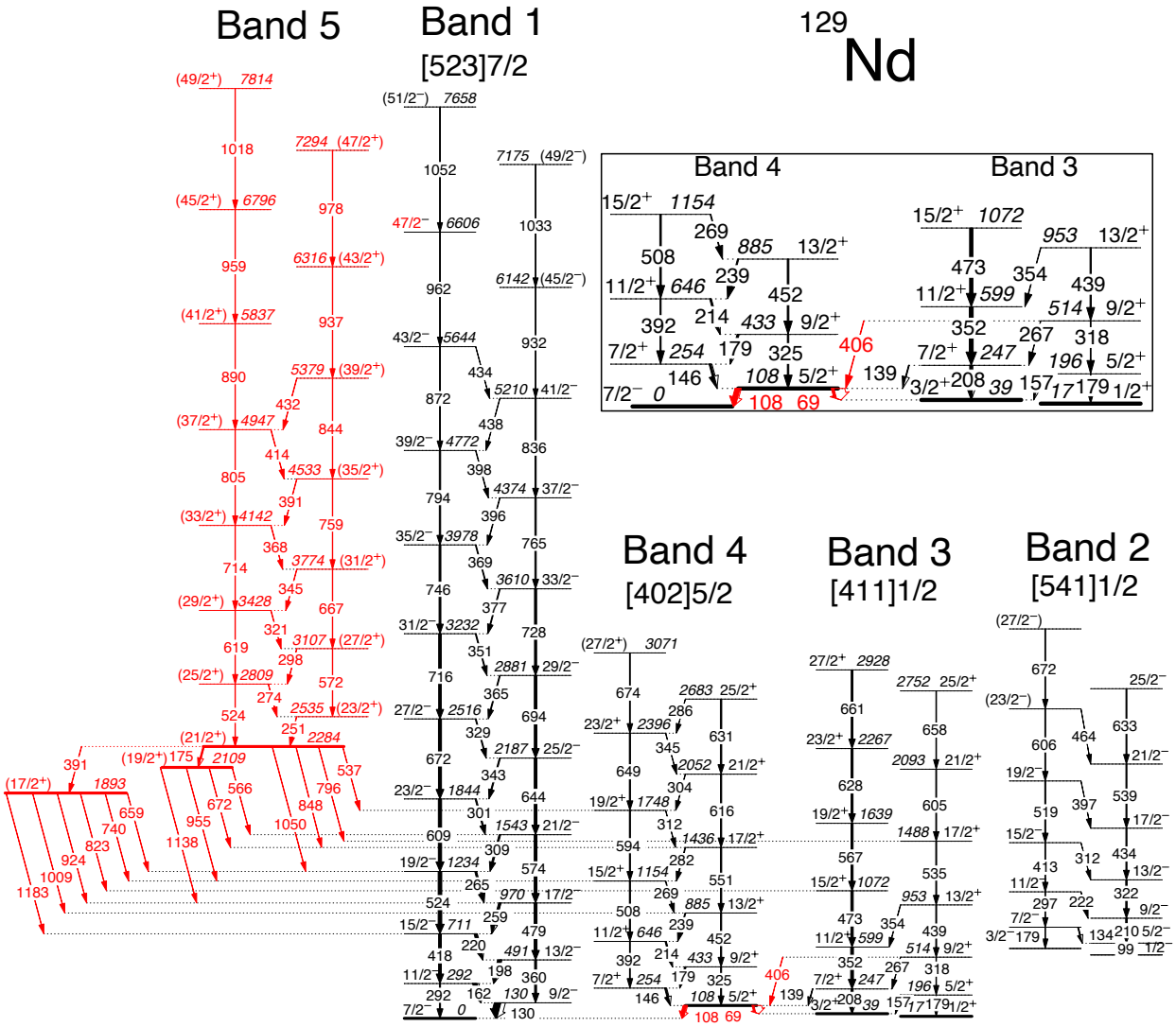

FIG. 1: Partial level scheme of ^{129}Nd showing the isomer and its decay towards the low-lying states. The new transitions are drawn in red, while transitions reported in the previous work of Zeidan *et al.* [29] are indicated in black. The levels with isomeric character are drawn with thick lines. Excited levels in Band 1 up to energies similar to the highest ones observed in Band 5 are included for comparison. The Nilsson configurations assigned to the bands in Ref. [29] are also indicated. The insert shows a zoom of the low-spin part of Bands 3 and 4.

bital, like $\pi 9/2^+[404]$ or $\pi 5/2^+[413]$, which by having the angular momenta perpendicular to the rotation axis have tiny contributions to $J^{(1)}$. The neutron has to be placed in a negative-parity orbital to get the positive parity of the isomer, which can only be $\nu 7/2^-[523]$. We therefore acknowledge two candidates for the three-quasiparticle configuration of the 2284-keV isomeric state, $\{\nu 7/2^-[523] \otimes \pi(9/2^+[404]5/2^-[532])\}_{21/2^+}$ and $\{\nu 7/2^-[532] \otimes \pi(9/2^+[404]3/2^-[541])\}_{19/2^+}$.

From the analysis of the $logF_W$ values of the depopulating transitions one conclude that both $19/2^+$ or $21/2^+$ assignments nicely fits the systematics of the $E2$, $M1$ and $E1$ transitions depopulating high-K isomers [38] for all transitions excepting the 175- and 391-keV ones. The 391-keV transition has higher hindrance for both $E2$ and $M1$ characters, whereas the 175-keV transition has higher hindrance only for $M1$ character. The high hindrances of these two transitions would be in agreement with the systematics of the high-K isomers only if $\Delta K \geq 3$, which would lead to too low spins for the isomers that in turn would decay to levels with spins higher by more than $2\hbar$ than that of the initial states, and therefore can be discarded. To explain the $logF_W$ values of the 175- and 391-keV transitions we have to invoke the presence of additional hindrances, which can be induced by very different configurations or different deformations of the isomers.

In order to further investigate the configuration of the

TABLE I: Energies (E_γ), spin and parity assignments ($I_i^\pi \rightarrow I_f^\pi$), relative intensities (T_γ), and mixing ratios (δ) of the $\Delta I = 1$ transitions in Band 5 above the $K^\pi = 21/2^+$ isomer, as well as the Weisskopf hindrance factors $logF_W$ of the transitions depopulating the $21/2^+$ isomer.

$E_\gamma(keV)^a$	$I_i^\pi \rightarrow I_f^\pi$	T_γ^b	δ	$logF_W$
Band 5				
250.6	$(23/2^+) \rightarrow (21/2^+)$	100	0.32(7)	
274.0	$(25/2^+) \rightarrow (23/2^+)$	61(3)	0.43(16)	
297.7	$(27/2^+) \rightarrow (25/2^+)$	38(3)	0.32(6)	
321.5	$(29/2^+) \rightarrow (27/2^+)$	33(3)	0.38(13)	
345.2	$(31/2^+) \rightarrow (29/2^+)$	19(3)		
368.1	$(33/2^+) \rightarrow (31/2^+)$	20(3)		
391.1	$(35/2^+) \rightarrow (33/2^+)$	11(2)		
413.5	$(37/2^+) \rightarrow (35/2^+)$	14(2)		
432.3	$(39/2^+) \rightarrow (37/2^+)$	5(2)		
523.9	$(25/2^+) \rightarrow (21/2^+)$	31(4)		
571.7	$(27/2^+) \rightarrow (23/2^+)$	32(4)		
619.2	$(29/2^+) \rightarrow (25/2^+)$	37(4)		
666.7	$(31/2^+) \rightarrow (27/2^+)$	42(4)		
713.8	$(33/2^+) \rightarrow (29/2^+)$	40(4)		
758.7	$(35/2^+) \rightarrow (31/2^+)$	39(4)		
804.7	$(37/2^+) \rightarrow (33/2^+)$	37(4)		
844.1	$(39/2^+) \rightarrow (35/2^+)$	31(4)		
890.4	$(41/2^+) \rightarrow (37/2^+)$	38(4)		
937(2)	$(43/2^+) \rightarrow (39/2^+)$	<10		
959(2)	$(45/2^+) \rightarrow (41/2^+)$	<10		
978(2)	$(47/2^+) \rightarrow (43/2^+)$	<10		
1018(2)	$(49/2^+) \rightarrow (45/2^+)$	<10		
Decay out from the $21/2^+$ isomer				
175.3	$(21/2^+) \rightarrow (19/2^+)$	15(2)		1.56(7)
391.0	$(21/2^+) \rightarrow (17/2^+)$	20(2)		3.29(8)
536.7	$(21/2^+) \rightarrow 19/2^+$	3(1)		7.70(2)
796.0	$(21/2^+) \rightarrow 17/2^+$	6(1)		5.62(18)
847.8	$(21/2^+) \rightarrow 17/2^+$	49(3)		4.47(5)
1049.8	$(21/2^+) \rightarrow 19/2^-$	7(1)		10.50(9)
Decay out from the $19/2^+$ isomer				
565.8	$(19/2^+) \rightarrow 21/2^-$	24(2)		
671.7	$(19/2^+) \rightarrow 17/2^+$	19(2)		
954.5	$(19/2^+) \rightarrow 15/2^+$	22(2)		
1138.4	$(19/2^+) \rightarrow 17/2^-$	35(2)		
Decay out from the $17/2^+$ isomer				
659.4	$(17/2^+) \rightarrow 19/2^-$	25(2)		
739.8	$(17/2^+) \rightarrow 15/2^+$	12(2)		
822.9	$(17/2^+) \rightarrow 15/2^-$	15(2)		
924.5	$(17/2^+) \rightarrow 17/2^-$	16(2)		
1009.1	$(17/2^+) \rightarrow 13/2^+$	10(2)		
1183.5	$(17/2^+) \rightarrow 15/2^-$	22(2)		

a The uncertainty on the transition energies is 0.2 keV for transitions below 1000 keV, and 0.5 keV for transitions above 1000 keV, except when indicated differently.

b Relative intensities corrected for efficiency, normalized to the intensity of the 250.6 keV transition for Band 5, and to 100% for the transitions depopulating each of the three isomers. The transition intensities were obtained from a combination of the total projection and gated spectra.

$21/2^+$ isomeric state, the mixing ratios of the $\Delta I = 1$ and $\Delta I = 2$ transitions depopulating a given state of spin I of the band built on the isomer have been estimated from the transition intensities employing standard formulae valid in the approximation of an axially symmetric rotating nucleus [39, 40]:

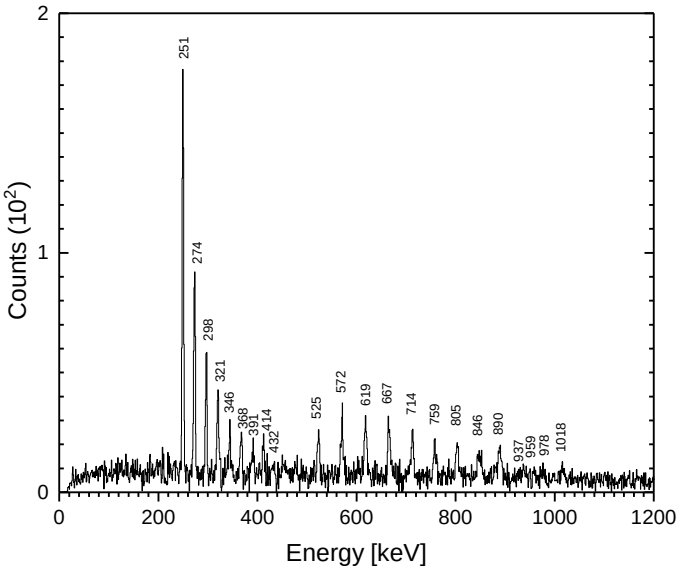

FIG. 2: Spectrum of γ-rays of Band 5 built on the $21/2^+$ isomeric state measured at the target position of the JUROGAM 3 array, obtained by employing the recoil gated isomer decay tagging technique on the 848-keV transition depopulating the isomer and on the 551-keV transition of Band 4 detected by the germanium detectors at the MARA focal plane.

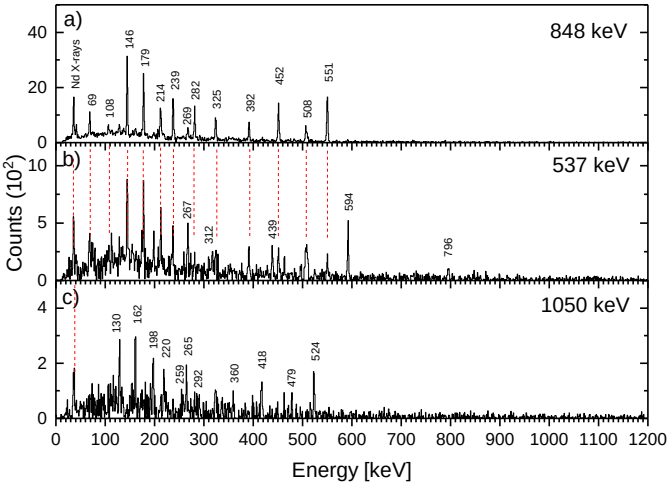

FIG. 3: $\gamma\gamma$-coincidence spectra of the delayed transitions measured at the MARA focal plane when gating on the a) 848-keV, b) 537-keV and c) 1050-keV transitions depopulating the $21/2^+$ isomeric state. The 267- and 439-keV transitions in panel b) are due to the feeding by the delayed 796-keV transition of the $17/2^+$ level of Band 3, which subsequently decays via the 535-keV transition, contaminating thus the 537-keV gate.

$$\frac{\delta^2}{1+\delta^2} = \frac{2K^2(2I-1)}{(I+1)(I-1+K)(I-1-K)} \frac{E_1^5}{E_2^5} \frac{T_2}{T_1}, \quad (1)$$

$$\frac{g_K - g_R}{Q_0} = \frac{0.933 E_1}{\delta\sqrt{(I^2-1)}}, \quad (2)$$

where δ is the mixing ratio, E is the transition energy

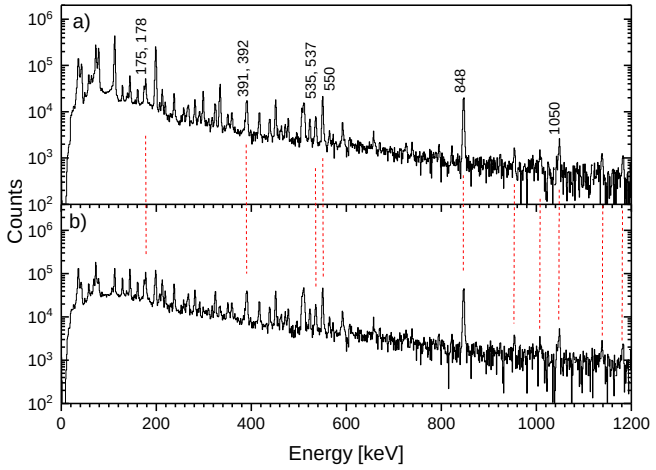

FIG. 4: a) Singles γ-ray spectrum and b) projection of the $\gamma\gamma$ coincidence matrix measured with the germanium detectors at the MARA focal plane, showing the ensemble of transitions depopulating the high-K isomers and the states of Bands 1, 3 and 4 of ^{129}Nd. The energies of the unlabeled transitions indicated with red lines are given in the text.

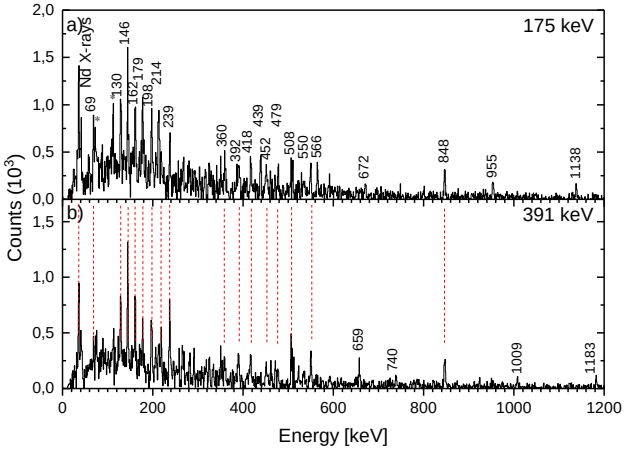

FIG. 5: Focal plane spectra from $\gamma\gamma$ coincidences gated on the 175- and 391-keV transitions from the $21/2^+$ isomer, showing the depopulating transitions of the $19/2^+$ and $17/2^+$ isomers to states of the Bands 1, 3 and 4. Contaminating transitions are indicated with asterisks.

in MeV, T is the γ-ray transition intensity, and Q_0 is in units of eb. The subscripts 1, 2 refer to $\Delta I = 1$, 2 transitions, respectively. The $\mid \delta \mid$ values can be estimated from Eq. (1) by assuming a certain K-value, whereas the sign of δ can be obtained from the analysis of the angular correlations of the emitted γ rays. From Eq. (1) one obtains $\mid \delta \mid \approx 0.5$. If the δ values are positive, the $(g_K - g_R)/Q_0$ values are also positive for a prolate shape [41]. To estimate g_K we can adopt a smaller gyromagnetic factor of $g_R = 0.3$ than the rotational approximation $g_R = Z/A = 0.46$, as suggested by that recently observed experimentally for the 8^- high-K isomer in ^{130}Ba, for which $g_R = 0.278(15)$ has been extracted instead of $g_R = Z/A = 0.43$ [42]. We can also adopt an intrinsic quadrupole moment of $Q_0 = 5.5$

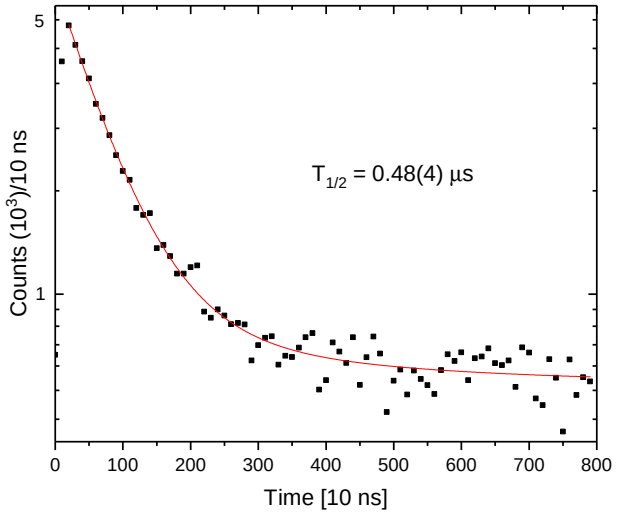

FIG. 6: Time spectrum and its fit with two exponentials from which the half-life of the $21/2^+$ isomeric state was determined. The spectrum is obtained with a start given by the recoils detected in the DSSD, and the stop given by the 848-keV transition depopulating the isomer and the 551-keV transition of Band 4 detected by the germanium detectors at the MARA focal plane.

eb corresponding to an axially symmetric prolate shape with a deformation of $\beta_2 = 0.3$, as suggested by the calculations. With this adopted values, one obtains a gyromagnetic factor of $g_K \approx 0.3 + \frac{0.11}{\delta} \approx 0.53$ for $I = 12.5$. Very similar values are obtained for higher spins. This has to be compared with calculated g_K values for different three-quasiparticle configurations, which are ≈ 0 for three-neutron configurations, and $\approx +1$ for one neutron-two proton configurations. One can therefore conclude that the configuration involving two protons is favored. This conclusion is also supported by the mixing ratios that could be extracted for the 251- and 298-keV transitions of Band 5, which are positive and around 0.36^{+23}_{-9} (see Table I), in fair agreement with the estimated absolute values extracted using the relations (1) and (2). For an oblate shape such a conclusion is not valid, but, as will be discussed in the following subsection, the oblate configuration can be safely discarded, because the calculated energy is too high and no minimum for an oblate shape is calculated in the potential energy surfaces.

The spin-parity of the 1893-keV state is fixed as $17/2^+$ by the 391-keV populating transition from the $21/2^+$ isomer and the 1009-keV depopulating transition to the $13/2^+$ state of Band 4 which have to be $E2$ otherwise one transition would be $\Delta I = 1$ and the other one $\Delta I = 3$ which is very unlikely. The spin-parity of the 2109-keV state is fixed as $19/2^+$ by the 955-keV transition to the $15/2^+$ state of Band 4, the 566-keV transition to the $21/2^-$ state of Band 1, and the 175-keV transition from the $21/2^+$ isomeric state. These assignments are also in agreement with the results of the calculations described in the following subsection. Very different configurations have to be chosen for the $19/2^+$ and $17/2^+$ isomeric

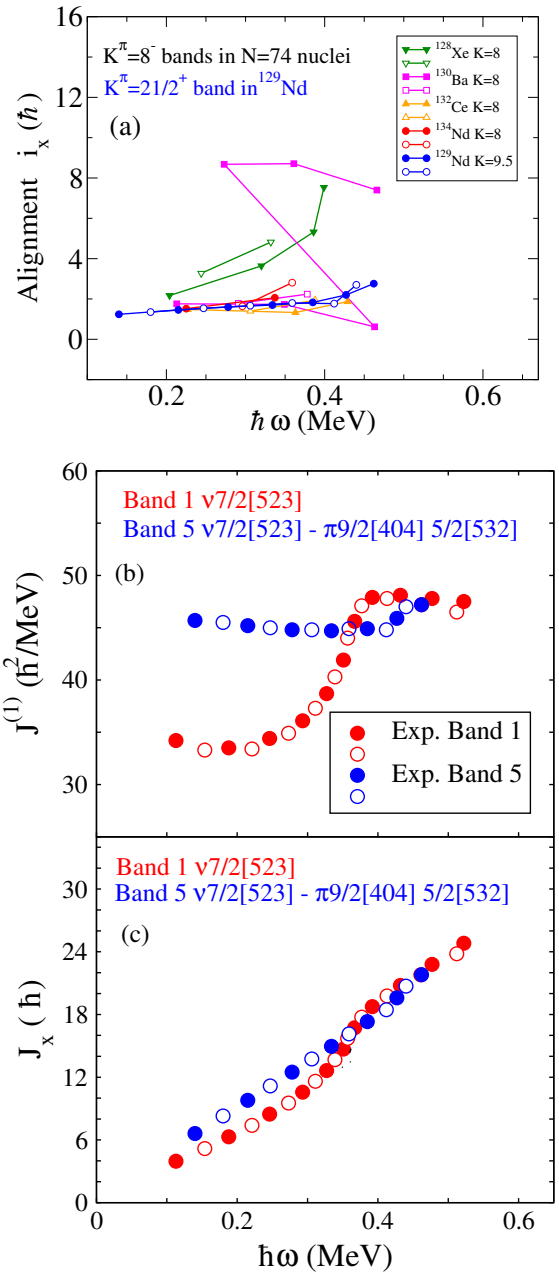

FIG. 7: a) Single-particle aligned angular momenta for the bands built on the $21/2^+$ isomer in ^{129}Nd and for the 8^- isomers in the $N = 74$ nuclei. The Harris parameters are $J^{(0)} = 14\ \hbar^2\ \mathrm{MeV}^{-1}$ and $J^{(2)} = 38\ \hbar^4\ \mathrm{MeV}^{-3}$for the $N = 74$ isomers, and $J^{(0)} = 38\ \hbar^2\ \mathrm{MeV}^{-1}$ and $J^{(2)} = 15\hbar^4\ \mathrm{MeV}^{-3}$ for the $21/2^+$ isomer in ^{129}Nd; b) experimental kinematic moments of inertia $J^{(1)}$; c) projections on the cranking axis of the total angular momentum J_x for Bands 1 and 5 of ^{129}Nd.

states, since no transition has been observed between them. This can be realized if we adopt the $\nu 7/2^-[523] \otimes \pi(5/2^+[413]5/2^-[532])$ configuration for the $17/2^+$ isomeric state, which differs by two proton and one neutron excitations from the $\nu 5/2^+[402] \otimes \pi(9/2^+[404]5/2^+[413])$ configuration assigned to the $19/2^+$ isomeric state. Moreover, this configuration is similar to the $\nu 7/2^-[523]$ $\otimes$

$\pi(9/2^+[404]5/2^-[532])$ configuration of the $21/2^+$ isomeric state, from which it differs by one proton excitation, being thus in agreement with the observation of the connecting 391-keV transition.

The $17/2^+$ and $19/2^+$ states at 1893 and 2109 keV, respectively, have decay patterns similar to those of the 2284-keV $21/2^+$ isomeric state, suggesting high-K configurations and isomeric character. Their half-lives could not be directly determined in the present experiment. For estimating their half-lives, we analyzed the Weisskopf hindrance factors $logF_W = log\frac{\tau_\gamma}{\tau_W}$ of the depopulating transitions (τ_γ is the partial γ-ray lifetime and τ_W is the Weisskopf estimate), which depend on the electromagnetic character of the transition and increase nearly linearly with ΔK [38]. It was found that they are compatible with high ΔK values ranging between 3 and 4 for half-lives of tens of nanoseconds, between 5 and 6 for half-lives of a few hundreds nanoseconds, and between 6 and 7 for half-lives of a few microseconds, giving support to their high-K nature. By imposing that the $logF_W$ values of the depopulating transitions are in agreement with the systematics [38], the best agreement was obtained for half-lives between several nanoseconds and tens of nanoseconds for both isomers. The decreasing half-lives of the three high-K isomers $21/2^+$, $19/2^+$ and $17/2^+$ can be partially related to their increasing energy relative to the yrast line.

The transitions from the isomer to the previously known bands fix the absolute energies of Bands 1, 3 and 4, and at the same time confirm the relative energies of Bands 3 and 4 established in Ref. [29]. A new 406-keV $E2$ transition from the $9/2^+$ state of Band 3 to the $5/2^+$ band-head of Band 4 has been identified, which confirms the assigned relative spins and positive parity of Bands 3 and 4 [29]. The present results provide evidence that the ground state of ^{129}Nd is $7/2^-$, the band-head of Band 1, not $5/2^+$, the band-head of Band 4, as presently adopted by ENSDF [43]. We found that the $5/2^+$ band-head of Band 4 decays via two delayed transitions of 69 and 108 keV to the $3/2^+$ state of Band 3 and the newly assigned $7/2^-$ ground state, respectively. These transitions have been observed at the focal plane of MARA in coincidence with the 848-keV transition depopulating the $21/2^+$ isomeric state, and also in delayed coincidence with the transitions of Band 4 below the $19/2^+$ state, the highest fed by depopulating transitions from the $21/2^+$ isomeric state. However, they were not observed in prompt coincidence with transitions of Band 4 above the $19/2^+$ level. This indicates that the $5/2^+$ band-head of Band 4 is isomeric, with a half-life of a few tens of nanoseconds. An indirect confirmation of the isomeric character of the 108-keV, $5/2^+$ state is the non-observation of the 69-keV transition in the previous experiment of Zeidan *et al.* [29], in which only prompt coincidences were measured. In the present experiment we also used a thin target, but unlike the Zeidan *et al.* experiment [29], we were able to observe the delayed 69- and 108-keV transitions emitted at the focal plane of the MARA separator due to the feeding of Band 4 by transitions from the long-lived $21/2^+$ isomeric state.

The lowest states of Band 3 with spins $1/2^+$ and $3/2^+$ have excitation energies of 17 and 39 keV, respectively. Their decays to the $7/2^-$ ground state via low-energy $E3$ and $M2$ transitions would be extremely hindered, they most probably β-decay with a half-life of $T_{1/2} = 2.6$ s, as proposed in Ref. [30].

Band 2 remains floating, as no connecting transitions from the $21/2^+$ isomeric state or to low-lying states have been identified. As Band 2 is the weakest among the four one-quasiparticle bands of ^{129}Nd [29], it is unlikely that its band head is close or lower than the $1/2^+, 3/2^+$ states of Band 3 towards it can decay. For this reason Band 2 is drawn in Fig. 1 more excited than the other bands.

Finally, it is worth noting that from the present experiment we did not find evidence of the $(7/2^-)$ isomer with half-life of $\approx$ 7 s proposed in the ENSDF compilation [43].

B. Theoretical calculations

In order to check if and to what extent the spin-parity and configuration assignments to the newly identified isomers is supported by various nuclear models, we performed several calculations. The deformations and excitation energies of the high-K isomers are summarized in Table II. The calculations with the three models CC-PES, PSM and PNC-CSM for the $\nu 7/2^-[523] \otimes (\pi 9/2^+[404]5/2^-[532])$ configuration assigned to the $21/2^+$ isomeric state are shown in Fig. 8.

As will be discussed in the following, all three employed models calculate the $21/2^+$ state lower in energy than the possible $19/2^+$ and $17/2^+$ states. Therefore, the natural spin-parity assignment for the 2284-keV isomeric state is $21/2^+$. However, one cannot simply discard the $19/2^+$ assignment without justification. There are two possible $19/2^+$ configurations, $\nu 7/2^-[523] \otimes \pi(9/2^+[404]3/2^-[541])$ and $\nu 5/2^+[402] \otimes \pi(9/2^+[404]5/2^+[413])$, which are calculated by CC-PES using the Wood-Saxon potential in an inverse order than that calculated by PSM and PNC-CSM using the Nilsson potential (see Table II). We therefore have to analyze two possible scenarios for the $19/2^+$ assignment to the 2284-keV isomeric state, one based on the order resulting from the CC-PES and PNC-CSM calculations, and one based on the order resulting from the PSM calculations. However, the $E2$ component of the 175-keV transition between the two $19/2^+$ configurations appears to be not additionally hindered in both scenarios, even though it would connect states with very different configurations. The $19/2^+$ assignment can therefore be discarded. The higher hindrance of the 175-keV transition, if of $M1$ character, can be explained if one selects the $\nu 5/2^+[402] \otimes \pi(9/2^+[404]5/2^+[413])$ configuration for the $19/2^+$ isomeric state, which differs by both neutron and proton single-particle excitations from that of the

$21/2^+$ isomeric state, leading to a low overlap between the wave functions (see the following discussion), while the higher hindrance of the 391-keV transition connecting states with configurations involving proton orbitals with different deformation driving forces ($\pi 9/2^+[404]$ towards higher deformation and $\pi 5/2^+[413]$ flat for prolate deformation) can be explained by the calculated different deformations of the $21/2^+$ ($\beta_2 = 0.31$) and $17/2^+$ ($\beta_2 = 0.28$) states (see Table II). The $21/2^+$ assignment corresponds in fact to the maximum spin that can be obtained with available orbitals around the proton and neutron Fermi surfaces for a prolate deformation of $\varepsilon_2 = 0.3$. In conclusion, we adopt the $21/2^+$ spin-parity and the $\nu 7/2^-[523] \otimes \pi(9/2^+[404]5/2^-[532])$ configuration for the $21/2^+$ isomeric state.

1. CC-PES calculations

First we performed CC-PES calculations to investigate if the isomers are based on oblate shapes. No minimum was found for oblate deformations for any configuration involving proton and neutron orbitals close to the Fermi surface. We therefore discarded the oblate shapes for the observed isomers. All possible one-quasiparticle and three quasiparticle configurations involving orbitals close to the Fermi surfaces for prolate deformations have been calculated, employing a Woods-Saxon potential and Lipkin-Nogami pairing [10]. For each quasiparticle configuration, the occupied orbitals were fixed and the deformation parameters $(\beta_2, \gamma, \beta_4)$ were varied in order to minimize the excitation energies. The neutron and proton monopole pairing strengths were determined by the average gap method [44]. The results of various one- and three-quasiparticle configurations are summarized in Table III. They all have nearly axially symmetric prolate shapes with deformations between $\beta_2 \approx 0.28$ and $\beta_2 \approx 0.32$, and moderate triaxialities between $-8°$ and $15°$. The lowest excited one-quasiparticle configurations, normalized to the lowest calculated one, are those assigned to Bands 1, 3 and 4: 0, 53 and 153 keV for Bands 1, 4 and 3, respectively, being in good agreement with the experimental energies which are in a narrow interval of ≈100 keV. Band 2 is calculated to be much more highly excited, at 1200 keV, which can thus explain its lower intensity [29] and the lack of observed connecting transitions with the other bands. The $\nu 7/2^-[523] \otimes \pi(9/2^+[404]5/2^-[532])$ configuration that we assign to the $21/2^+$ isomeric state is calculated at 2.605 MeV, and has a nearly axially symmetric prolate shape with $\beta_2 = 0.31$ and $\gamma = -4°$ (see Fig. 8a). The three-quasiparticle candidate configurations for the $17/2^+$ and $19/2^+$ isomeric states are calculated at higher energies and slightly smaller deformations than those of the $21/2^+$ isomeric state.

2. PSM calculations

The structure of the one-quasiparticle bands has also been investigated using the PSM, using slightly different quadrupole deformations than those suggested by the CC-PES calculations. Results of the calculations for Bands 1, 2, 3 and 4, adopting $\varepsilon_2 = 0.29$ and $\varepsilon_4 = 0.02$ taken from Ref. [45], are shown in Fig. 9. Both the energies and the observed signature staggering below the upbending are nicely reproduced in all bands, which are essential prerequisites for obtaining good agreement for the three-quasiparticle configurations. The bands have been calculated up to very high excitation energy, to investigate their evolution with increasing spin. The ground state with $I^\pi = 7/2^-$ is reproduced, which is different from Ref. [29]. The band-head energies for Bands 3 and 4 are well described with PSM, as 19 keV (17 keV) and 192 keV (108 keV) respectively. For the floating Band 2, the PSM gives 785 keV as the band-head energy. The states with spin lower than about 23/2 are reproduced nicely, including the energies and signature staggering, while some discrepancies show up for Bands 2 and 4 at high spin. Band 1 is well described up to the highest spin 75/2, where 5-qp configurations are found to be important.

One important conclusion resulting from the PSM calculations is that the possible oblate configuration $\nu 5/2^+[402] \otimes (\pi 5/2^+[402]9/2^-[514])$ is calculated higher relative to the prolate $\nu 7/2^-[402] \otimes (\pi 9/2^+[404]5/2^-[532])$ configuration, and with definitely larger curvature of the E versus J and corresponding smaller moment of inertia $J^{(1)}$ (see Fig. 10), which corroborates the results of the CC-PES calculations, inducing us to confidently assign the configuration built on the prolate shape for the $21/2^+$ isomeric state. One can note the following weak points of the PSM results, due to the assumed axial deformation, which however have no impact on the isomer interpretation: a lower signature staggering both before the upbending and at the highest observed spins in Band 1, opposite staggering at the bottom and after the upbending in Band 2, a slightly lower staggering in Band 3, and opposite staggering in Band 4 above the upbending.

3. PNC-CSM calculations

The PNC-CSM calculations give reasonably good results for Bands 1, 3 and 4, but failed to reproduce the observed gradual upbending in the positive signature partner for Band 2 (see Fig. 11). Three quasiparticle configurations have also been calculated. Two of them are shown in Fig. 8b, where one can see that $J^{(1)}$ of the $\nu 7/2^-[523] \otimes (\pi 9/2^+[404]5/2^-[532])$ configuration assigned to the $21/2^+$ isomeric state is calculated closest to the experimental one over a large frequency interval. However, the calculated splitting between the signature partners at high frequency is not observed in the exper-

TABLE II: Calculated energies of the assigned configurations to the three high-K isomers. The configurations are given in terms of Nilsson quantum numbers. The shape parameters (β_2, γ) resulting form the CC-PES calculations, as well as the adopted quadrupole deformations ε_2 for the PNC-CSM and PSM calculations are also indicated. The approximate relation between β_2 and ε_2 is $\varepsilon_2 \approx 0.95 * \beta_2$.

I^π	$E_x^{exp}(keV)$	$Configuration$	$CC-PES\ (\beta_2,\gamma)$	$PNC\text{-}CSM\ (\varepsilon_2)$	$PSM\ (\varepsilon_2)$
$21/2^+$	2284	$\nu 7/2^-[523]\pi 9/2^+[404]5/2^-[532]$	2605 $(0.31, -4°)$	3272 (0.31)	2247 (0.35)
$19/2^+$	2109	$\nu 7/2^-[523]\pi 9/2^+[404]3/2^-[541]$	3016 $(0.29, -6°)$	4973 (0.29)	3195 (0.35)
$19/2^+$	2109	$\nu 5/2^+[402]\pi 9/2^+[404]5/2^+[413]$	3210 $(0.29, -8°)$	3992 (0.29)	2786 (0.35)
$17/2^+$	1893	$\nu 7/2^-[523]\pi 5/2^+[413]5/2^-[532]$	3044 $(0.28, 0°)$	2421 (0.28)	2836 (0.35)
$17/2^+$	1893	$\nu 5/2^+[402]\pi 9/2^+[404]3/2^+[411]$	2702 $(0.30, 9°)$	4658 (0.30)	3092 (0.35)

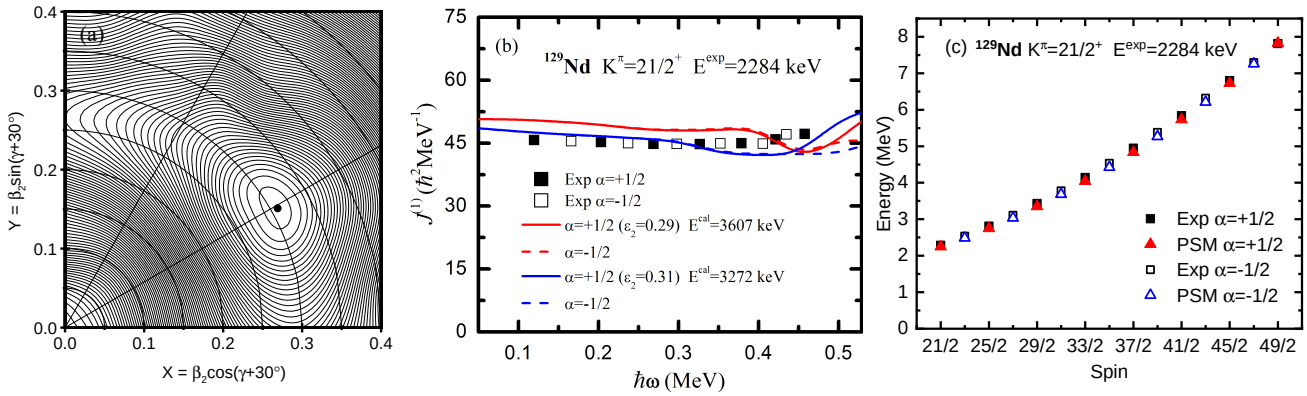

FIG. 8: Calculations for the $\nu 7/2^-[523] \otimes \pi(9/2^+[404]5/2^-[532])$ configuration assigned to the $21/2^+$ isomeric state: a) Potential energy surface calculated with the CC-PES model; b) Comparison between the experimental kinematic moment of inertia $J^{(1)}$ of Band 5 built on the $21/2^+$ isomeric state and the PNC-CSM calculations; the experimental data are denoted by solid and open squares, while the PNC-CSM results are drawn with solid and dashed lines for signature $\alpha = +1/2$ and $\alpha = -1/2$, respectively. c) Comparison between the experimental Band 5 built on the $21/2^+$ isomeric state and the PSM calculations, using deformation parameters $\varepsilon_2 = 0.35$ and $\varepsilon_4 = 0.02$ which best reproduce the band-head and level energies.

iment. A larger deformation can reproduce better the $J^{(1)}$ values, but the inherent lowering of the $\nu 1/2^-[541]$ intruder and its interaction with the negative-parity $h_{11/2}$ orbitals induces an unobserved perturbation at high frequency.

Table IV shows the results of the PNC-CSM calculations of one- and three-quasiparticle configurations in ^{129}Nd. The deformation parameters are taken from Möller and Nix's Table of 1995 [46]. To reproduce better the experimental band-head energies, some of them are adopted from the CC-PES calculated deformations in Table 2. In particular, the deformation $\varepsilon_2 = 0.310$ is adopted for the newly observed band built on the 2284-keV isomer, which leads to a good agreement with both of the experimental state energy and the kinematic moment of inertia shown in Fig. 8b. This suggests that for excited multi-quasiparticle configurations the CC-PES calculated deformations can be better than the Möller and Nix ones.

IV. SUMMARY

In summary, the present study of ^{129}Nd, the lightest isotope known spectroscopically in the odd-even neodymium sequence, lead to the identification of three high-K isomers and one low-spin isomer, as well as the reassignment of the ground state spin-parity to $7/2^-$. This is the first observation of a three-quasiparticle isomer in the $A \approx 130$ mass region close to the proton drip line. From the analysis of the transitions depopulating the $21/2^+$ isomeric state we extracted its half-life, while from the analysis of the Weisskopf hindrance factors of the depopulating transitions we tentatively assigned the spin-parity. From the analysis of the band built on the isomer combined with the results of CC-PES, PSM and PNC-CSM calculations we assigned three-quasiparticle prolate configurations involving one neutron and two protons to all three high-K isomers. The present results represent the first example of high-K isomers involving the $\pi 9/2^+[404]$ orbital in nuclei with Z well above the $Z = 50$ shell closure, suggesting the existence of such isomers in other nuclei close to the proton drip line in the $A \approx 130$ mass region, which hopefully will be discovered in the future.

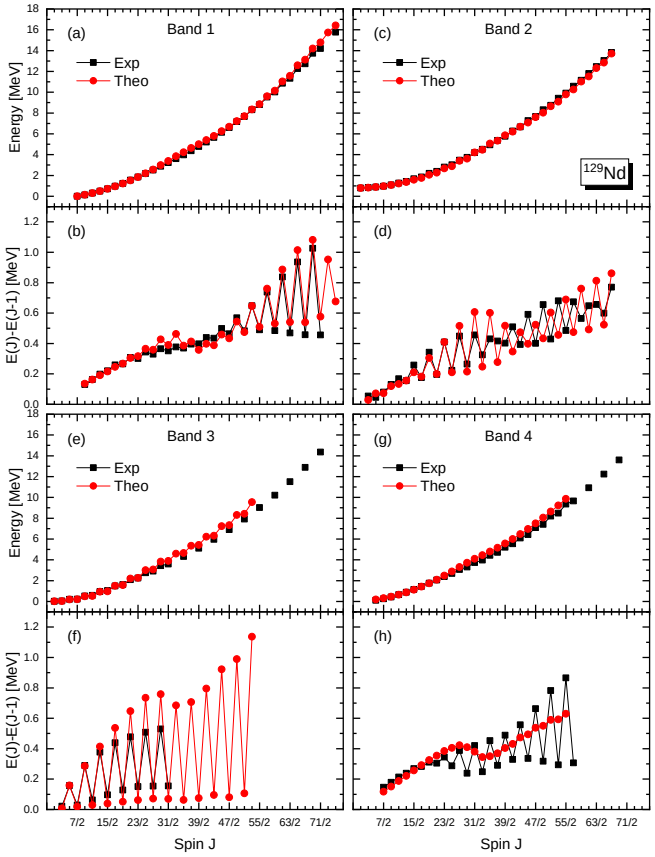

FIG. 9: Results of PSM calculations [11] for Bands 1, 2, 3, and 4 of ^{129}Nd, adopting $\varepsilon_2 = 0.29$ and $\varepsilon_4 = 0.02$ taken from Ref. [45], in comparison with the data of this work and those from Ref. [29].

V. ACKNOWLEDGEMENTS

This work has been supported by the United Kingdom Science and Technology Facilities Council through grants ST/P004598/1 and ST/V001027/1; by the National Natural Science Foundation of China under grant No. U2032138; by the Special Research Assistant Project of the Chinese Academy of Sciences; by the Academy of Finland under the Finnish Centre of Excellence Programme (2012-2017); by the EU 7th Framework Programme Project No. 262010 (ENSAR). The use of germanium detectors from the GAMMAPOOL is acknowledged.

[1] J. Sarén *et al.*, Nucl. Instr. Meth. Phys. Res. A **266**, 4196 (2008), URL https://doi.org/10.1016/j.nimb.2008.05.027.
[2] J. Uusitalo, J. Sarén, J. Partanen, and J. Hilton, Acta Phys. Pol. B **50**, 319 (2019).
[3] J. Pakarinen *et al.*, Eur. Phys. J. A **56**, 149 (2020).
[4] K. K. Zheng *et al.*, Physics Letters B **822**, 136645 (2021), ISSN 0370-2693, URL https://www.sciencedirect.com/science/article/pii/S0370269321005852.
[5] K. K. Zheng *et al.*, Phys. Rev. C **104**, 044305 (2021), URL https://link.aps.org/doi/10.1103/PhysRevC.104.044305.
[6] K. K. Zheng *et al.*, Phys. Rev. C **104**, 044325 (2021).
[7] K. K. Zheng *et al.*, Phys. Rev. C **104**, 014326 (2021).
[8] K. K. Zheng *et al.*, Eur. Phys. J. A **58**, 50 (2022), URL https://doi.org/10.1140/epja/s10050-022-00704-y.
[9] B. F. Lv *et al.*, Phys. Rev. C **105**, 044319 (2022), URL https://doi.org/10.1103/PhysRevC.105.044319.
[10] F. R. Xu, P. M. Walker, J. A. Sheikh, and R. Wyss, Physics Letters B **435**, 257 (1998), ISSN 0370-2693, URL https://www.sciencedirect.com/science/article/pii/S0370269398008570.
[11] K. Hara and Y. Sun, International Journal of Modern Physics E **04**, 637 (1995), URL https://www.worldscientific.com/doi/abs/10.1142/S0218301395000250.
[12] J. Y. Zeng, T. H. Jin, and Z. J. Zhao, Phys. Rev. C **50**, 1388 (1994), URL https://doi.org/10.1103/PhysRevC.50.1388.
[13] B. H. Smith *et al.*, Physics Letters B **443**, 89 (1998), URL https://www.sciencedirect.com/science/article/pii/s3702693989013379.
[14] J. Blachot, Nuclear Data Sheets **111**, 1471 (2010).
[15] J. Blachot, Nuclear Data Sheets **113**, 2391 (2010).
[16] J. Blachot, Nuclear Data Sheets **95**, 679 (2002).
[17] D. M. Symochko, E. Browne, and J. K. Tuli, Nuclear Data Sheets **110**, 2945 (2009).
[18] S. Ohya, Nuclear Data Sheets **111**, 1619 (2010).
[19] J. Chen, Nuclear Data Sheets **174**, 1 (2021).
[20] J. Katakura, Nuclear Data Sheets **112**, 495 (2011).
[21] A. Hashizume, Nuclear Data Sheets **112**, 1647 (2011).
[22] C. M. Petrache *et al.*, Eur. Phys. J. A **12**, 139 (2001).
[23] O. Zeidan *et al.*, Phys. Rev. C **66**, 044311 (2019).
[24] D. J. Hartley *et al.*, Phys. Rev. C **63**, 024316 (2001).
[25] D. J. Hartley *et al.*, Phys. Rev. C **61**, 044328 (2000).
[26] B. H. Smith *et al.*, Physics Letters B **415**, 223 (1997),

TABLE III: Table with the results of the CC-PES calculations for different configurations involving orbitals around the neutron and proton Fermi surfaces of ^{129}Nd.

Nuclei	Configurations	β_2	$\gamma(^\circ)$	β_4	E_x^{cal} (keV)
^{129}Nd-1qp					
	$\nu\frac{7}{2}^-[523]$	0.304	0	0.002	0
	$\nu\frac{5}{2}^+[402]$	0.314	0	0.017	53
	$\nu\frac{1}{2}^+[411]$	0.309	0	0.010	150
	$\nu\frac{5}{2}^+[413]$	0.318	0	0.013	715
	$\nu\frac{1}{2}^-[541]$	0.295	0	-0.004	1200
	$\nu\frac{7}{2}^+[404]$	0.278	1	0.016	1509
	$\nu\frac{9}{2}^-[514]$	0.279	0	0.018	3329
^{129}Nd-3qp					
$\frac{13}{2}^-$	$\nu\frac{5}{2}^+[402]\otimes\pi\frac{3}{2}^-[541]\otimes\pi\frac{5}{2}^+[413]$	0.271	0	-0.003	2701
$\frac{15}{2}^-$	$\nu\frac{7}{2}^+[404]\otimes\pi\frac{3}{2}^-[541]\otimes\pi\frac{5}{2}^+[413]$	0.267	8	0.002	3657
$\frac{15}{2}^-$	$\nu\frac{5}{2}^+[402]\otimes\pi\frac{5}{2}^+[413]\otimes\pi\frac{5}{2}^-[532]$	0.289	0	0.011	3122
$\frac{15}{2}^-$	$\nu\frac{7}{2}^-[523]\otimes\pi\frac{5}{2}^+[413]\otimes\pi\frac{3}{2}^+[411]$	0.272	1	-0.012	2629
$\frac{15}{2}^-$	$\nu\frac{7}{2}^-[523]\otimes\nu\frac{7}{2}^+[404]\otimes\nu\frac{1}{2}^+[411]$	0.289	0	0.029	1752
$\frac{17}{2}^-$	$\nu\frac{5}{2}^+[402]\otimes\pi\frac{9}{2}^+[404]\otimes\pi\frac{3}{2}^-[541]$	0.278	15	0.013	3209
$\frac{19}{2}^-$	$\nu\frac{7}{2}^+[404]\otimes\pi\frac{9}{2}^+[404]\otimes\pi\frac{3}{2}^-[541]$	0.287	12	0.028	3223
$\frac{19}{2}^-$	$\nu\frac{7}{2}^-[523]\otimes\nu\frac{5}{2}^+[413]\otimes\nu\frac{7}{2}^+[404]$	0.281	0	0.020	3325
$\frac{19}{2}^-$	$\nu\frac{5}{2}^+[413]\otimes\nu\frac{5}{2}^+[402]\otimes\nu\frac{9}{2}^-[514]$	0.289	0	0.021	5230
$\frac{19}{2}^-$	$\nu\frac{5}{2}^+[402]\otimes\nu\frac{7}{2}^+[404]\otimes\nu\frac{7}{2}^-[523]$	0.279	0	0.028	2776
$\frac{19}{2}^-$	$\nu\frac{7}{2}^-[523]\otimes\pi\frac{9}{2}^+[404]\otimes\pi\frac{3}{2}^+[411]$	0.295	6	0.007	2751
$\frac{19}{2}^-$	$\nu\frac{5}{2}^+[402]\otimes\pi\frac{9}{2}^+[404]\otimes\pi\frac{5}{2}^-[532]$	0.317	6	0.020	2525
$\frac{19}{2}^-$	$\nu\frac{1}{2}^+[404]\otimes\pi\frac{9}{2}^+[404]\otimes\pi\frac{3}{2}^-[541]$	0.287	12	0.028	3223
$\frac{13}{2}^+$	$\nu\frac{5}{2}^+[402]\otimes\pi\frac{5}{2}^+[413]\otimes\pi\frac{3}{2}^+[411]$	0.265	-5	-0.007	2993
$\frac{15}{2}^+$	$\nu\frac{7}{2}^-[523]\otimes\pi\frac{3}{2}^-[541]\otimes\pi\frac{5}{2}^+[413]$	0.284	0	-0.012	2231
$\frac{17}{2}^+$	$\nu\frac{7}{2}^-[523]\otimes\pi\frac{5}{2}^+[413]\otimes\pi\frac{5}{2}^-[532]$	0.284	0	0.008	3044
$\frac{17}{2}^+$	$\nu\frac{5}{2}^+[402]\otimes\pi\frac{9}{2}^+[404]\otimes\pi\frac{3}{2}^+[411]$	0.301	9	0.016	2702
$\frac{19}{2}^+$	$\nu\frac{7}{2}^-[523]\otimes\pi\frac{9}{2}^+[404]\otimes\pi\frac{3}{2}^-[541]$	0.288	-6	0.000	3016
$\frac{19}{2}^+$	$\nu\frac{5}{2}^+[402]\otimes\pi\frac{9}{2}^+[404]\otimes\pi\frac{5}{2}^+[413]$	0.293	-8	0.013	3210
$\frac{21}{2}^+$	$\nu\frac{7}{2}^-[523]\otimes\pi\frac{9}{2}^+[404]\otimes\pi\frac{5}{2}^-[532]$	0.310	-4	0.016	2605

URL https://www.sciencedirect.com/science/article/pii/S0370269397012458.

[27] D. Bazzacco *et al.*, Phys. Rev. C **58**, 2002 (1998).

[28] H.-L. Liu and F.-R. Xu, Chinese Phys. Lett. **25**, 1621 (2008), URL https://iopscience.iop.org/article/10.1088/0256-307X.

[29] O. Zeidan *et al.*, Phys. Rev. C **65**, 024303 (2002).

[30] S. W. Xu *et al.*, Eur. Phys. J. A **55**, 58 (2010).

[31] D. M. Cullen *et al.*, Phys. Rev. C **58**, 846 (1998).

[32] G. Duchêne *et al.*, Nucl. Instr. Meth. Phys. Res. A **432**, 90 (1999), URL https://doi.org/10.1016/S0168-9002(99)00277-6.

[33] C. W. Beausang *et al.*, Nucl. Instr. Meth. Phys. Res. A **313**, 37 (1992), URL https://doi.org/10.1016/0168-9002(92)90084-H.

[34] J. Hilton *et al.*, Phys. Rev. C **100**, 014305 (2019).

[35] P. Rahkila, Nucl. Instrum. Meth. Phys. Res. A **595**, 637 (2008), URL https://doi.org/10.1016/j.nima.2008.08.039.

[36] D. Radford, Nucl. Instrum. Meth. Phys. Res. A **361**, 297 (1995), ISSN 0168-9002, URL http://www.sciencedirect.com/science/article/pii/0168900295001832.

[37] D. Radford, Nucl. Instrum. Meth. Phys. Res. A **361**, 306 (1995), ISSN 0168-9002, URL http://www.sciencedirect.com/science/article/pii/0168900295001840.

[38] F. G. Kondev, G. D. Dracoulis, and T. Kibédi, Atomic Data and Nuclear Data Tables **103-104**, 50 (2015).

[39] G. B. Hagemann *et al.*, Phys. Rev. C **25**, 3224(R) (1982).

[40] N. J. Stone, R. J. Stone, P. M. Walker, and C. R. Bingham, Physics Letters B **726**, 675 (2013).

[41] F. R. Xu, P. M. Walker, J. A. Sheikh, and R. Wyss, Physics Letters B **34**, 269 (1970), URL https://www.sciencedirect.com/science/article/pii/0370269371906009.

[42] Y. H. Qiang *et al.*, Phys. Rev. C **99**, 014307 (2019).

[43] J. Timar, Z. Elekes, and B. Singh, Nuclear Data Sheets **121**, 143 (2014).

[44] P. Möller and J. R. Nix, Nucl. Phys. 1 **536**, 20 (1992), URL https://doi.org/10.1016/0375-9474(92)90244-E.

[45] P. Möller, A. J. Sierk, T. Ichikawa, and H. Sagawa, Atomic Data and Nuclear Data Tables **109-110**, 1 (2016), URL https://doi.org/10.1016/j.adt.2015.10.002.

[46] P. Möller, J. R. Nix, W. D. Myers, and W. J. Swiatecki, Atomic Data and Nuclear Data Tables **59**, 185 (1995), URL https://doi.org/10.1016/adnd.1995.1002.

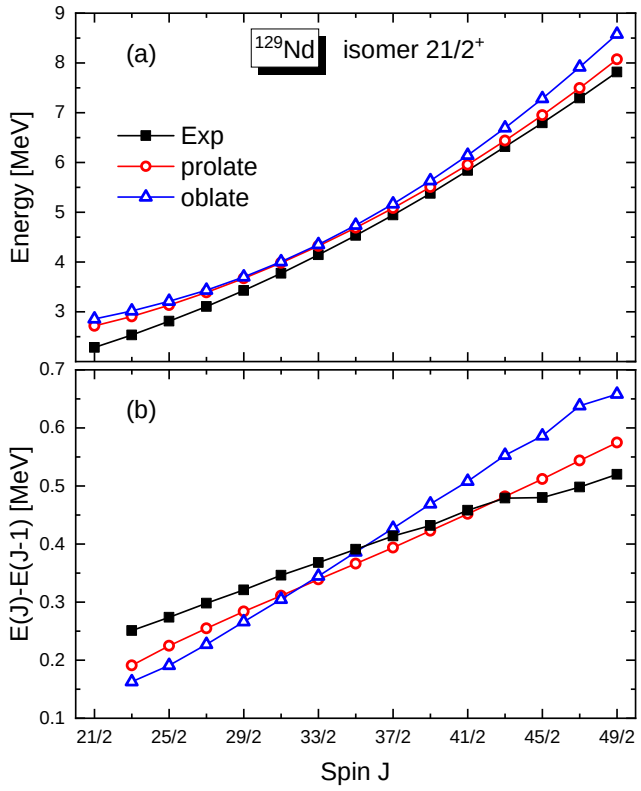

FIG. 10: Calculated $E(J)$ and $E_\gamma = E(J) - E(J-1)$ values for Band 5 in ^{129}Nd with the projected shell model [11], assuming prolate and oblate shapes, with deformation parameters $\varepsilon_2 = \pm 0.30$ and $\varepsilon_2 = 0.04$.

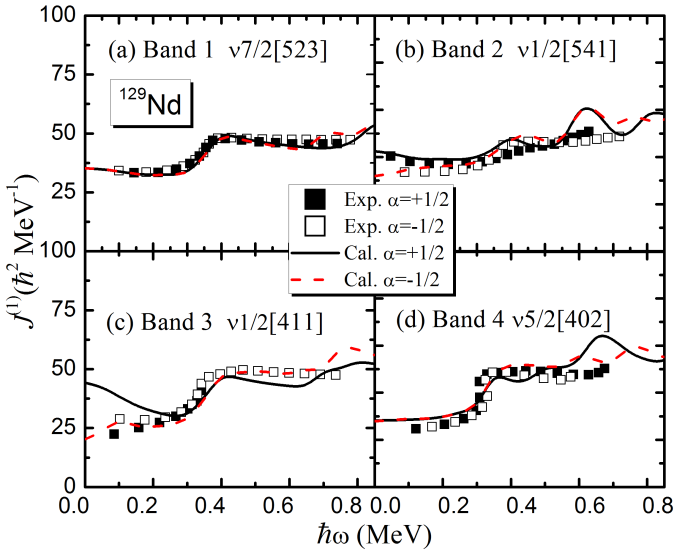

FIG. 11: Comparison of the kinematic moment of inertia $\mathcal{J}^{(1)}$ calculated with PNC-CSM and the experimental data for Bands 1, 2, 3 and 4 in ^{129}Nd.

TABLE IV: Results of the PNC-CSM calculations of one- and three-quasiparticle configurations in ^{129}Nd.

K^π	Configuration	ε_2	ε_4	ε_6	E_x^{cal}(keV)	E_x^{exp}(keV)
$\frac{7}{2}^-$	$\nu\frac{7}{2}^-[523]$	0.292	0.070	-0.002	0	0
$\frac{1}{2}^+$	$\nu\frac{1}{2}^+[411]$	0.292	0.070	0.000	902	22
$\frac{5}{2}^+$	$\nu\frac{5}{2}^+[402]$	0.292	0.040	-0.002	915	108
$\frac{1}{2}^-$	$\nu\frac{1}{2}^-[541]$	0.292	0.000	-0.002	433	133
$\frac{5}{2}^+$	$\nu\frac{5}{2}^+[413]$	0.292	0.033	-0.002	1536	
$\frac{5}{2}^-$	$\nu\frac{5}{2}^-[532]$	0.292	0.033	-0.002	1456	
$\frac{7}{2}^+$	$\nu\frac{7}{2}^+[404]$	0.292	0.033	-0.002	1632	
$\frac{3}{2}^+$	$\nu\frac{3}{2}^+[411]$	0.292	0.033	-0.002	2176	
$\frac{9}{2}^-$	$\nu\frac{9}{2}^-[514]$	0.292	0.033	-0.002	2218	
$\frac{15}{2}^+$	$\nu\frac{7}{2}^-[523]\otimes\pi\frac{3}{2}^+[411]\otimes\pi\frac{5}{2}^-[532]$	0.292	0.033	-0.002	3293	
	$\nu\frac{1}{2}^+[411]\otimes\pi\frac{5}{2}^+[413]\otimes\pi\frac{9}{2}^+[404]$	0.292	0.033	-0.002	3724	
	$\nu\frac{5}{2}^-[532]\otimes\pi\frac{5}{2}^+[413]\otimes\pi\frac{5}{2}^-[532]$	0.292	0.033	-0.002	4108	
	$\nu\frac{1}{2}^-[541]\otimes\pi\frac{5}{2}^-[532]\otimes\pi\frac{9}{2}^+[404]$	0.292	0.033	-0.002	4941	
	$\nu\frac{7}{2}^+[404]\otimes\pi\frac{3}{2}^+[411]\otimes\pi\frac{5}{2}^+[413]$	0.292	0.033	-0.002	5227	
$\frac{15}{2}^-$	$\nu\frac{1}{2}^-[541]\otimes\pi\frac{5}{2}^+[413]\otimes\pi\frac{9}{2}^+[404]$	0.320	0.033	-0.001	3094	
	$\nu\frac{5}{2}^+[402]\otimes\pi\frac{5}{2}^+[413]\otimes\pi\frac{5}{2}^-[532]$	0.292	0.033	-0.002	3447	
	$\nu\frac{7}{2}^-[523]\otimes\pi\frac{3}{2}^+[411]\otimes\pi\frac{5}{2}^+[413]$	0.292	0.033	-0.002	3565	
	$\nu\frac{1}{2}^+[411]\otimes\pi\frac{5}{2}^-[532]\otimes\pi\frac{9}{2}^+[404]$	0.292	0.033	-0.002	4173	
$\frac{17}{2}^+$	$\nu\frac{7}{2}^-[523]\otimes\pi\frac{5}{2}^+[413]\otimes\pi\frac{5}{2}^-[532]$	0.280	0.033	-0.001	2421	1893
	$\nu\frac{5}{2}^+[402]\otimes\pi\frac{9}{2}^+[404]\otimes\pi\frac{3}{2}^+[411]$	0.300	0.033	-0.001	4658	
	$\nu\frac{3}{2}^+[411]\otimes\pi\frac{5}{2}^+[413]\otimes\pi\frac{9}{2}^+[404]$	0.292	0.033	-0.002	5441	
	$\nu\frac{9}{2}^-[514]\otimes\pi\frac{3}{2}^+[411]\otimes\pi\frac{5}{2}^-[532]$	0.292	0.033	-0.002	5535	
$\frac{17}{2}^-$	$\nu\frac{7}{2}^+[404]\otimes\pi\frac{5}{2}^+[413]\otimes\pi\frac{5}{2}^-[532]$	0.292	0.033	-0.002	4222	
	$\nu\frac{5}{2}^-[532]\otimes\pi\frac{3}{2}^+[411]\otimes\pi\frac{9}{2}^+[404]$	0.292	0.033	-0.002	5410	
	$\nu\frac{3}{2}^+[411]\otimes\pi\frac{5}{2}^-[532]\otimes\pi\frac{9}{2}^+[404]$	0.292	0.033	-0.002	5889	
$\frac{19}{2}^+$	$\nu\frac{5}{2}^+[402]\otimes\pi\frac{5}{2}^+[413]\otimes\pi\frac{9}{2}^+[404]$	0.290	0.033	-0.001	4064	2109
	$\nu\frac{5}{2}^+[413]\otimes\pi\frac{5}{2}^+[413]\otimes\pi\frac{9}{2}^+[404]$	0.29	0.033	-0.001	4642	
	$\nu\frac{9}{2}^-[514]\otimes\pi\frac{5}{2}^+[413]\otimes\pi\frac{5}{2}^-[532]$	0.292	0.033	-0.002	4801	
	$\nu\frac{7}{2}^-[523]\otimes\pi\frac{9}{2}^+[404]\otimes\pi\frac{3}{2}^-[541]$	0.292	0.033	-0.002	4973	
	$\nu\frac{5}{2}^-[532]\otimes\pi\frac{5}{2}^-[532]\otimes\pi\frac{9}{2}^+[404]$	0.292	0.033	-0.002	5172	
$\frac{19}{2}^-$	$\nu\frac{7}{2}^-[523]\otimes\pi\frac{3}{2}^+[411]\otimes\pi\frac{9}{2}^+[404]$	0.292	0.033	-0.002	3874	
	$\nu\frac{5}{2}^+[402]\otimes\pi\frac{9}{2}^+[404]\otimes\pi\frac{5}{2}^-[532]$	0.292	0.033	-0.002	4512	
	$\nu\frac{5}{2}^+[413]\otimes\pi\frac{9}{2}^+[404]\otimes\pi\frac{5}{2}^-[532]$	0.292	0.033	-0.002	5091	
$\frac{21}{2}^+$	$\nu\frac{7}{2}^-[523]\otimes\pi\frac{9}{2}^+[404]\otimes\pi\frac{5}{2}^-[532]$	0.310	0.033	-0.001	3272	2284